Accepted Manuscript

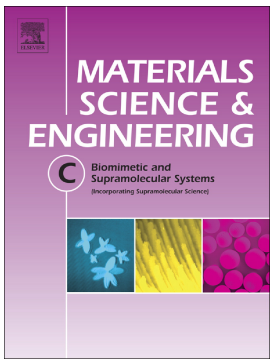

Complementary approaches for the evaluation of biocompatibility of 90Y-labeled superparamagnetic citric acid (Fe,Er)3O4 coated nanoparticles

Bratislav Antic, Marko Boskovic, Jasmina Nikodinovic-Runic, Yue Ming, Hongguo Zhang, Emil S. Bozin, Drina Janković, Vojislav Spasojevic, Sanja Vranjes-Djuric

PII: S0928-4931(16)32050-1
DOI: doi: 10.1016/j.msec.2017.02.023
Reference: MSC 7354

To appear in: *Materials Science & Engineering C*

Received date: 4 November 2016
Revised date: 30 November 2016
Accepted date: 6 February 2017

Please cite this article as: Bratislav Antic, Marko Boskovic, Jasmina Nikodinovic-Runic, Yue Ming, Hongguo Zhang, Emil S. Bozin, Drina Janković, Vojislav Spasojevic, Sanja Vranjes-Djuric , Complementary approaches for the evaluation of biocompatibility of 90Y-labeled superparamagnetic citric acid (Fe,Er)3O4 coated nanoparticles. The address for the corresponding author was captured as affiliation for all authors. Please check if appropriate. Msc(2016), doi: 10.1016/j.msec.2017.02.023

Complementary Approaches for the Evaluation of Biocompatibility of ^{90}Y-labeled Superparamagnetic Citric Acid $(Fe,Er)_3O_4$ Coated Nanoparticles

Bratislav Antic[1,*], Marko Boskovic[1], Jasmina Nikodinovic-Runic[2], Yue Ming[3,**], Hongguo Zhang[3], Emil S. Bozin[4], Drina Janković[1], Vojislav Spasojevic[1] and Sanja Vranjes-Djuric[1]

[1] Vinča Institute of Nuclear Sciences, University of Belgrade, P. O. Box 522, 11001 Belgrade, Serbia

[2] Institute of Molecular Genetics and Genetic Engineering, University of Belgrade, Vojvode Stepe 444a, 11010 Belgrade, Serbia

[3] College of Materials Science and Engineering, Beijing University of Technology, Pingleyuan 100, Chaoyang District, Beijing 100124, P. R. China

[4] Condensed Matter Physics and Materials Science Department, Brookhaven National Laboratory, Upton, NY 11973, USA

*Corresponding author: Email, bantic@vinca.rs

**Corresponding author: Email, yueming@bjut.edu.cn

Abstract

Magnetic nanoparticles (MNPs) are of immense interest for diagnostic and therapeutic applications in medicine. Design and development of new iron oxide-based MNPs for such applications is of rather limited breadth without reliable and sensitive methods to determine their levels in body tissues. Commonly used methods, such as ICP, are quite problematic, due to the inability to decipher the origin of the detected iron, i.e. whether it originates from the MNPs or endogenous from tissues and bodily fluids. One of the approaches to overcome this problem and to increase reliability of tracing MNPs is to partially substitute iron ions in the MNPs with Er. Here, we report on the development of citric acid coated $(Fe,Er)_3O_4$ nanoparticles and characterization of their physico-chemical and biological properties by utilization of various complementary approaches. The synthesized MNPs had a narrow (6-7 nm) size distribution, as consistently seen in atomic pair distribution function, transmission electron microscopy, and DC magnetization measurements. The particles were found to be superparamagnetic, with a pronounced maximum in measured zero-field cooled magnetization at around 90 K. Reduction in saturation magnetization due to incorporation of 1.7% Er^{3+} into the Fe_3O_4 matrix was clearly observed. From the biological standpoint, citric acid coated $(Fe,Er)_3O_4$ NPs were found to induce low toxicity both in human cell fibroblasts and in zebrafish (*Danio rerio*) embryos. Biodistribution pattern of the MNPs after intravenous administration in healthy Wistar rats was followed by the radiotracer method, revealing that ^{90}Y-labeled MNPs were predominantly found in liver (75.33% ID), followed by lungs (16.70% ID) and spleen (2.83% ID). Quantitative agreement with these observations was obtained by ICP-MS elemental analysis using Er as the detected tracer. Based on the favorable physical, chemical and biological characteristics, citric acid coated $(Fe,Er)_3O_4$ MNPs could be further considered for the potential application as a

diagnostic and/or therapeutic agent. This work also demonstrates that combined application of these techniques is a promising tool for studies of pharmacokinetics of the new MNPs in complex biological systems.

KEYWORDS: Magnetic nanoparticle, Biodistribution, Embryotoxicity, Radiolabeling, MNP

1. Introduction

Magnetic nanoparticles (MNPs) are currently being intensively investigated due to their wide range of possible applications in different branches of technology [1].The field of medicine offers numerous opportunities for improvement of diagnostics and therapy using MNPs. The most promising medical applications of MNPs are in magnetic resonance imaging, drug delivery and as heating agents in magnetic hyperthermia [2-6]. In order to be used for medical applications, MNPs should be biocompatible, with suitable magnetic properties, narrow size distribution, as well as having chemical stability.

The only FDA approved magnetic material that can be used in human therapy so far is magnetite (Fe_3O_4) [7]. Nevertheless, applications of different methodologies for MNP detection *in vivo* [8] are scarce. One of the greatest challenges to that effect is reliably quantifying the biodistribution of exogenous iron oxide based nanoparticles in the presence of the background signal originating from very abundant endogenous iron ions. Usually, the distribution and accumulation of MNPs in different organs is evaluated using a combination of several techniques, including magnetic resonance imaging, *X*-ray fluorescence and X-ray absorption [9]. Elemental analysis based on inductively coupled plasma optical emission (*ICP-OES*) and mass spectrometry (*ICP-MS*) is a frequently used method for studying both pharmacokinetics and biodistribution [10]. Although ICP-MS has a rather high sensitivity for detecting iron, it is not

reliable as a MNP-specific tracer, since iron is found in abundance in all biological fluids and tissues in the forms of hemoglobin, ferritin, and myoglobin. The problem is potentiated in the case of detecting iron content in the liver, since this organ is not only the target organ for nanoparticles (>200 *nm*), but is also the storage organ for iron (the proteins, ferritin and hemosiderin). Ferritin is the major form of iron storage with a capacity of about 4500 iron (III) ions per protein molecule [11].

One possible way to overcome difficulties in studying the biodistribution of Fe_3O_4 nanoparticles is to partially substitute Fe cations with *4f* elements, which are not typically found in living organisms [12]. This could circumvent the large systematic errors occurring due to the inability to distinguish the origin of Fe. From a structural point of view, magnetite crystallizes in the cubic spinel type structure, space group (*S.G.*) $Fd\bar{3}m$. In this structure, cations occupy two different non-equivalent crystallographic positions (8*b* and 24*d*). Partial Fe cation substitution with *4f* rare earth (RE) elements in the spinel structure facilitates enhancement or alteration of the magnetic properties by changing the chemical composition of the compound. Due to appreciable ionic size mismatch between the host and dopant RE, associated structural distortions exert considerable crystallite strain [13]. Erbium has a large magnetic moment and high magnetic anisotropy, thereby potentially influencing the physical properties of the parent compound [13]. One of the concepts behind this study was to prepare magnetite nanoparticles, in which a proportion of the iron ions was substituted with erbium.

Information about the pharmacokinetics and biodistribution patterns of newly designed MPNs can be also obtained using a radiotracer technique [14,15]. Distribution of radiolabeled MNPs following intravenous administration is determined by measuring radioactivity in tissues and/or organs. Given the concerns pertaining to the radioactive character of the probe, limitations

are prescribed to minimize animal exposure to radioactivity, while at the same time allowing a statistically sufficient number of counts to be collected from the studied specimens. Therefore, the radiation doses from the tracer, even when a beta emitting tracer such as ^{90}Y is used, neither produce any detectable radiation damage nor invoke detectable responses from the studied specimens that would alter the results. In addition, the amount of radioactive label, in the chemical form given to the animal under study, must not alter the physiological functions of the organism.

In order to examine the reliability of these methodologies for biodistribution studies, $(Fe,Er)_3O_4$ citric acid (CA) coated nanoparticles were firstly synthesized and characterized. The microstructural properties of the MNPs were studied and their magnetic properties were determined. Physicochemical characterization was followed by investigation of cytotoxicity as well as embryotoxicity of the MNPs. Through the radiolabeling of prepared samples, several important aspects were addressed: i) optimization of the radiolabeling protocol, ii) investigation of *in vitro* and *in vivo* stability of the radiolabeled MNPs and iii) determination of the biodistribution of the radiolabeled MNPs. Finally, for the precise determination of the MNP levels in tissues, a parallel approach was used: a combination of radiotracer and *ICP* methods.

2. Experimental

2.1. Sample preparation

Ferrofluids based on CA coated $Fe_{3-x}Er_xO_4$ nanoparticles, where x=0 and 0.05 (further denoted by Er00 and Er05, respectively), were prepared via the modified Massart's method [16]. In a typical synthesis, 1.5 *M* NaOH was added dropwise to the initial solution with the stoichiometric ratio of $FeSO_4$·7H2O, $FeCl_3$·$6H_2O$, and $Er(NO_3)_3$. After reaching *pH* 10, the

suspension was heated to 80 *ºC* with vigorous stirring for 30 min. The co-precipitate was subjected to magnetic separation and rinsed repeatedly in deionized water to achieve neutral *pH*. CA-coated MNPs were obtained by initiating and conditioning the coating reaction until a stable suspension was established. Finally, the MNP suspension was centrifuged and washed several times with deionized water to rid it of any excess citric acid.

2.2. Physical characterization

TGA analyses were performed (30–700 *ºC* range) on a *SDT Q600 TGA/DSC* instrument (*TA* Instruments, USA), by utilizing a 20 *ºC/min* heating rate on less than 10 mg of sample. *TGA* was employed in order to determine the mass contribution of CA in dry MNPs. The CA content in Er00 and Er05 MNPs was found to be 18% and 11.5% of the mass, respectively.

Synchrotron experiments were conducted at 300 *K* on two samples of $Fe_{3-x}Er_xO_4$ with nominal compositions of x=0 (Er00) and 0.05 (Er05). Experiments were carried out at the X17A beam line of the National Synchrotron Light Source (NSLS) at Brookhaven National Laboratory (Upton, NY, USA) using a monochromatic x-ray beam with wavelength of 0.1839 *Å* (E=67.42 *keV*). Each sample was loaded into a polyimide capillary (1 mm in diameter) that was mounted 205.67 *mm* away from the Perkin Elmer amorphous silicon image plate detector positioned perpendicular to the beam path. Data was collected over multiple frames of 60 *s* each, which were further averaged for good statistics. Two-dimensional diffraction patterns were integrated, using *Fit2D* software, into their one-dimensional counterparts. These were corrected for various experimental effects, and the corresponding reduced total scattering functions, $F(Q)$, where Q is the momentum transfer, were then Sine Fourier transformed into the direct space to obtain the atomic pair distribution functions, *PDF* and $G(r)$. Data reduction was carried out using

PDFgetX3 software, with Q_{MAX}=24 $Å^{-1}$,which was optimized for minimizing the signal to noise ratio and maximizing the *r*-space resolution.

Magnetic and TEM measurements were obtained using standard equipment and under standard conditions. Magnetic measurements of powder MNPs were performed on a *MPMS XL-5 SQUID* magnetometer. Magnetization vs. temperature, *M (T)*, was measured in the temperature range 2–300 *K* under zero-field-cooled (*ZFC*) and field-cooled (*FC*) regimes, in 100 Oe. Hysteresis loops were measured at 5 *K* and 300 *K* in a *ZFC* regime. Transmission electron micrographs and selected-area diffraction patterns were collected with a transmission electron microscope (*JEM 2100 TEM*, Jeol, USA) operating at 200 *kV*.

2.3. *In vitro* cell studies: Antiproliferative activity assessed by *MTT* assay

Human lung fibroblast (*MRC5*) and melanoma (*A375*) cell lines were obtained from the ATCC culture collection and maintained and cultured as instructed by ATCC. In order to test cytotoxic effects, cells were maintained as monolayers (1x 10^4 cells $well^{-1}$) and grown in a humidified atmosphere of 95% air and 5% CO_2 at 37 °*C*.

The viability of cells was evaluated using the 3-(4,5-dimethylthiazol-2-yl)-2,5-diphenyltetrazolium bromide (*MTT*) reduction assay [17].This assay was carried out after 48 h of cell incubation in appropriate media containing test compounds (Er05 and Fe_3O_4 naked MNPs) at different concentrations and cell viability was measured as described [17]. Prepared 18 *nm in size* naked Fe_3O_4 MNPs were used as a control for the coated MNPs in toxicity studies. Er05 and Fe_3O_4 solutions in deionized water were filter sterilized (0.2 *μm*, EMD Millipore, Billerica, USA) prior to usage in the cell culture experiments. The results were presented as percentage of viability of the control, untreated cells (arbitrarily set to 100%). IC_{50} values were calculated as

concentrations at which 50% cell growth inhibition occurred. Experiments were conducted in hexaplicate in three independent determinations. Results are presented as means ± *SD*.

The morphological appearance of the treated cells was determined using a DM IL LED Inverted Microscope (Leica Microsystems, Wetzlar, Germany) under 20×magnification.

2.4. Embryotoxicity studies: Zebrafish (*Danio rerio*) toxicity assay

The assessment of toxicity (lethality and teratogenicity) of Er05 MNPs on zebrafish embryos was performed following the general rules of the OECD Guidelines for the Testing of Chemicals [18]. Adult zebrafish (*Danio rerio*, wild type) were obtained from a commercial supplier (Pet Centar, Belgrade, Serbia) and maintained in fish medium (2 *mM* $CaCl_2$, 0.5 *mM* $MgSO_4$, 0.7 *mM* $NaHCO_3$, 0.07 *mM* KCl) at 27 ± 1°*C*under a 14 *h* light/10 h dark cycle, and regularly fed twice daily with commercially dry flake food supplemented with *Artemianauplii* (TetraMin^{TM} flakes; Tetra Melle, Germany). Collected eggs at the 4- to 16-cellstages were individually treated with different concentrations of MNPs (5, 10 or50 *μg/ml*) after being transferred into 96-well plates containing 200 *μl* of MNP test solution and one egg per well. The study was repeated two times using 32 embryos per MPN concentration. Er05 and Fe_3O_4MNPsin deionized water were filter sterilized (0.2 *μm*, EMD Millipore, Billerica, USA) prior to usage in the zebrafish embryo experiments. Apical endpoints (Table S1) were examined and recorded 24, 48, 72, 96 and 114 h post fertilization (hpf) using an inverted microscope (CKX41; Olympus, Tokyo, Japan).

All studies involving zebrafish were performed in compliance with the European directive 86/609/*EEC* and the ethical guidelines given in the Guide for Care and Use of

Laboratory Animals, Institute for Molecular Genetics and Genetic Engineering, University of Belgrade.

2.5. Radiolabeling of Er05MNPs with ^{90}Y and *in vitro* stability studies

$^{90}YCl_3$ was purchased from Polatom, Poland, in a no-carrier-added form (29.64 *GBq/cm*^{3}, in 0.05 *M* HCl, 18.5 *TBq/mg* Y, according to the product specification).

^{90}Y labeling of Er05 MNPs was performed using the method previously applied for the radiolabeling of Fe_3O_4/PEG600diacid MNPs [19].Briefly, $^{90}YCl_3$ solution (5 *μl*, containing approximately 370 *MBq*) was added to an aqueous suspension of 30 *mg/ml*Er05 MNPs at *pH* 6.5. The suspension was shaken for 1 *h*. Radiolabeled Er05 MNPs were then recovered by magnetic decantation, the supernatant was removed and the precipitate washed several times with deionized water to eliminate any unbound $^{90}Y^{3+}$. The labeling yield was determined as the ratio of the measured MNP-associated activity obtained after magnetic separation and the known activity used for the radiolabeling. Formation of ^{90}Y-labeled Er05 MNPs and radiochemical purity were verified by instant thin layer chromatography performed on *SG* strips (*ITLC-SG*, glass microfiber chromatography paper impregnated with a silica gel) with saline as the mobile phase. With this system, ^{90}Y-labeled Er05 MNPs remained at the origin (R_f=0.0-0.1), while unbound ^{90}Y migrated with the solvent front (R_f=0.9-1.0).

The bremsstrahlung of ^{90}Y radioactivity was measured using a CRC-15 beta radioisotope dose calibrator (Capintec, USA) and a NaI (Tl) well-type gamma counter (Wizard 2480, Perkin Elmer, USA). All measurements were carried out under the same geometric conditions. The results are reported as the mean of at least three measurements ± standard deviation.

The stability of ^{90}Y-labeled Er05 MNPs during 72*h* was determined after magnetic precipitation or *ITLC-SG* with saline as the mobile phase. Amounts (3 *mg*;0.1 *ml*) of ^{90}Y-labeled Er05 MNPs were incubated with 1 *ml* of either saline or human serum at 37°*C*. After 3 days of incubation, radiolabeled particles were precipitated with a permanent magnet and the activity was measured separately in a 0.1 *ml* aliquot of the supernatant and in the remaining sample (radiolabeled MNPs and 0.9 *ml* supernatant). The radioactivity bound to ^{90}Y-labeled Er05 MNPs was calculated as follows: the activity of the remainder – the activity of the 0.1 *ml* supernatant x 0.9.

2.6. Biodistribution of ^{90}Y-labeled Er05 MNPs

The biodistribution study was performed according to the guidelines of the European Council Directive (86/609/*EEC*) and the Serbian Laboratory Animal Science Association (SLASA). Three healthy male 4-week-old Wistar rats (100±10 g body weight, Institute of Biology, Vinča Institute of Nuclear Sciences) received 0.1 *ml* of^{90}Y-labeled Er05MNPs (0.3 *mg* in saline, approx. 2.5 *MBq)* intravenously (i.v.) injected through the tail vein. The animals were sacrificed via spinal cord dislocation at 30 *min* after injection. Samples of blood and organs of interest were excised and weighed, then tissues were homogenized (Bio Spec Products, Inc., Bartlesville, USA) and diluted to a final volume of 5 *ml* with water to reach identical geometry and similar probe density. The percentage of injected dose (%*ID/g*) per gram of organ was calculated by comparing the activities with appropriate standards for injected dose (*ID*). The data are presented as average $\pm$ standard deviation from each group.

2.7. Elemental analysis by *ICP-MS*

Digestion of the samples for *ICP* measurements was performed on an Advanced Microwave Digestion System (*ETHOS 1*, Milestone, Italy) using a *HPR-1000/10S* high pressure segmented rotor. Pressure-resistant *PTFE* vessels (volume 100 ml) which were equipped with *QS-50* Quartz inserts were used. This type of vessel permitted a maximum temperature of 240 *ºC* and a maximum pressure of 100 *bar* to be applied. Sample digestion was performed as follow: whole organs of Wistar rats for biodistribution studies or zebrafish in case of ecotoxicity analysis were precisely weighed and mixed in quartz inserts with 5 ml HNO_3 (65%, Suprapure®, Merck, Germany) and then heated with microwave energy. The temperature was controlled with a predetermined power program. Digestion was conducted for 20 *min* at a constant temperature of 200 *ºC*, with a prior warm-up linearly over 10 *min* to 200 *ºC*. After total mineralisation and cooling to room temperature and without filtration, the solutions were diluted to a fixed volume in 10 *ml* volumetric flasks with ultra-pure water (Barnstead™ GenPure™ Pro, Thermo Scientific, Germany) with a conductivity of 0.055 *µS/cm*. The content of Er in digested sample solutions was determined by *ICP-MS* using an *iCAP Qc ICP-MS* (Thermo Scientific, Bremen, Germany) spectrometer with the operational software *Qtegra*. For Er determination, the spectrometer was adjusted for optimal performance in standard mode using the supplied auto tune protocols. The *ICP-MS* spectrometer was tuned using the solution *TUNE B iCAPQ* (1 µg/l of each: Ba, Bi, Ce, Co, In, Li, U), provided by the manufacturer (Thermo Scientific, Germany). Reference standard solutions for spectrometer calibration were prepared on the basis of the certified Semi quantitative Standard 1, Specpure® (Alfa Aesar GmbH & Co KG, Germany). Er determinations were done measuring two stable naturally occurring erbium isotopes,^{166}Er and ^{167}Er, and the average valueswere used for further calculations.The limit of quantitation (*LOQ*) for erbium was determined to be 11 *ng/l*.

3. Results and discussion

3.1. Structure and microstructure analysis

Analysis of collected synchrotron XRD data showed that Er00 and Er05 crystallized in the *S.G.* $Fd\bar{3}m$ and spinel structure type (Figure 1). Structural modeling of the PDF data was carried out using the *PDFFIT2*program operated under the *PDFGui* platform using *S.G.* $Fd\bar{3}m$ and spinel structure type. Er was assumed to occupy an octahedral 16d position within the spinel structure type. The Er content could not be independently verified for the Er-containing materials due to inter-parameter correlations within the modeling protocols used, so the Er content was considered to be the nominal Er-concentration and octahedral site occupancy. However, the presence of Er in the spinel structure was seen through small but observable changes in the lattice parameter of the spinel phase, which did not depend on the unit cell content. The lattice parameter of the spinel lattice depends on the complex interplay between the size of the ions and their distribution. Ionic radii for octahedral (VI) coordination are Fe^{3+}(VI) = 0.645 *Å*, while Er^{3+}(VI) = 0.89 *Å*[20].Further verification of the presence of Er on the octahedral spinel sites originated from the increased isotropic displacement parameters of octahedral sites and oxygen sublattices, which were enlarged for the Er05 sample as compared to the Er00 sample. Final fits of *PDF* data are shown in Figure 2. Small discrepancies between the model and the data in the low-*r* part of the *PDF* were consistently seen in both materials studied, and are likely attributable

to surface effects as well as those of strain related to the finite particle size. Exploring these structural effects in greater detail is beyond the scope of this study.

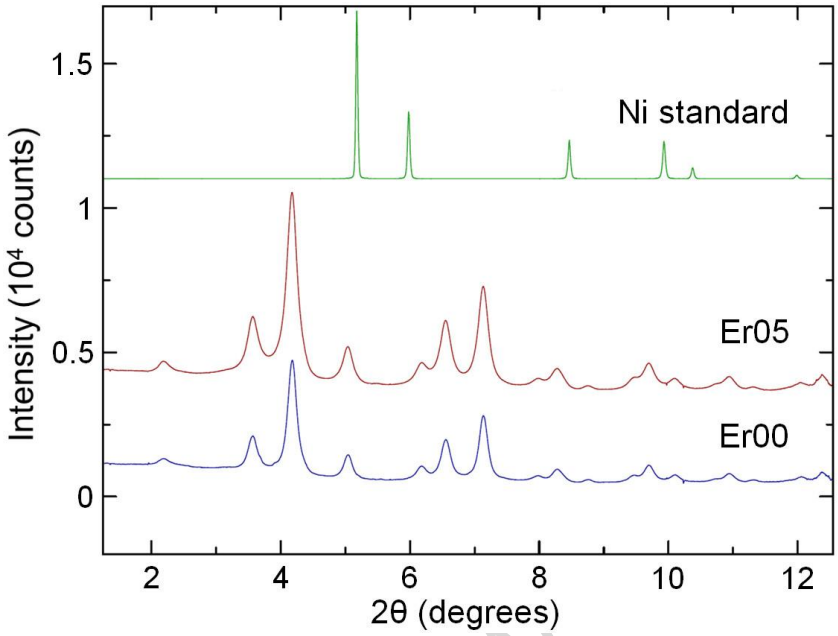

Figure 1. Diffraction patterns obtained in far detector setup (medium-high resolution mode), at 300 K for Ni standard (top, green profile), Er05 (middle, red profile), and Er00 (bottom, blue profile). Sharp Bragg peaks are obtained for the standard, illustrating the measurement resolution. Dramatically broader profiles are observed for Er00 and Er05, indicating their nanoscale character.

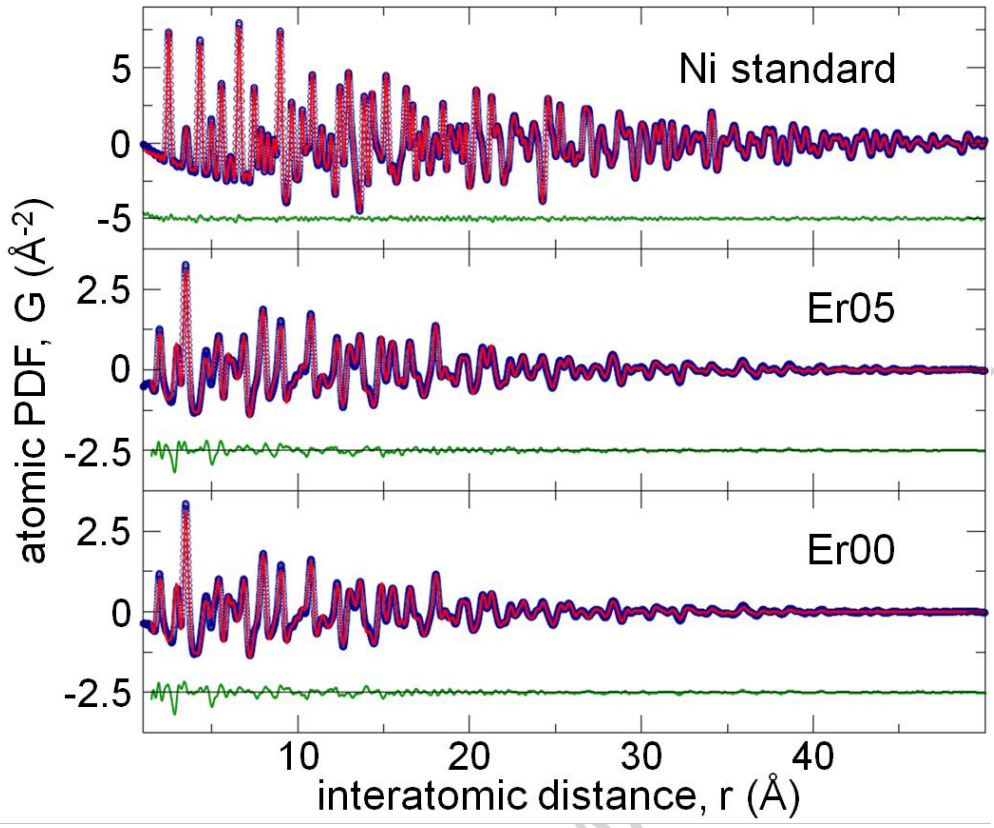

Figure 2. Experimental atomic PDFs (open symbols) with converged structural models (solid red lines) and associate difference curves (green, offset for clarity) for Ni standard (top), Er05 (middle), and Er00 (bottom) materials. Data for MNPs were fitted using a spinel Fd-3m model. PDF intensity is clearly observable in the of bulk Ni standard data at 50 Angstroms, whereas the intensity is clearly washed out for the MNPs studied, indicating loss of structural coherence and the nanoscale character of Er00 and Er05.

Structural parameters resulting from the *PDF* refinements for the principal spinel phase, obtained over the 1.5*Å*-50 *Å* fitting range, are summarized in Table 1.

MNP	*a (Å)*	*Fe-t Uiso ($Å^2$)*	*Fe-o Uiso ($Å^2$)*	*O Uiso ($Å^2$)*	*d (nm)*	r_{wp}
Er00	8.355(4)	0.007(2)	0.018(3)	0.022(4)	6.5(7)	0.16
Er05	8.364(4)	0.008(2)	0.020(3)	0.025(4)	5.3(4)	0.18

Table 1. Structural parameters for the principal spinel ($Fd\bar{3}m$) phase of the MNPs: lattice parameter, a, Isotropic atomic displacement parameter, Uiso, for Fe in tetrahedral (Fe-t) and Fe

in octahedral (Fe-o) positions, as well as oxygen. Fits, assuming spherical MNP shape also give particle diameter, d in nanometers. Finally, fit residuals r_{wp} give an indication of the goodness of fit.

The microstructure of the MNPs was further examined by *TEM* analysis. *TEM* images (Figure 3) of both MNP types were analyzed using image processing software, Image J [21]. Results of the particle counts are given in the insets. Both histograms resemble log-normal size distributions. Average diameters deduced from the count data were 7(2) and 6(1) *nm*, for Er00 and Er05, respectively. In comparison with the *X*-ray analysis, crystallite size was close to the size of the particles. This indicated that the materials were indeed MNPs, were comprised of single crystallites, and were nearly spherical in shape according to the morphological analysis conducted.

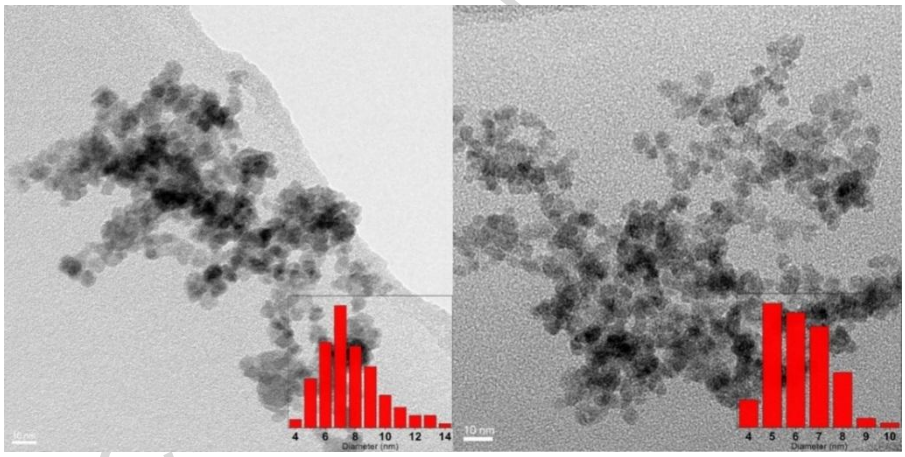

Figure 3. TEM images of Er00 (left) and Er05 (right) MNPs. Inset: Particle counts. Scale bar is 10 nm in both pictures.

3.2. Magnetic behavior

Figure 4 shows *ZFC-FC* curves for both MNP types. Both Er00 and Er05 exhibited behavior typical for superparamagnetic samples, with maximum magnetization around 90 *K* and overlapping *ZFC* and *FC* curves at higher temperatures. The slight rise of the *FC* curves with

temperature decreases below the maximum points to the presence of interparticle interactions, which is expected for powder samples [22].

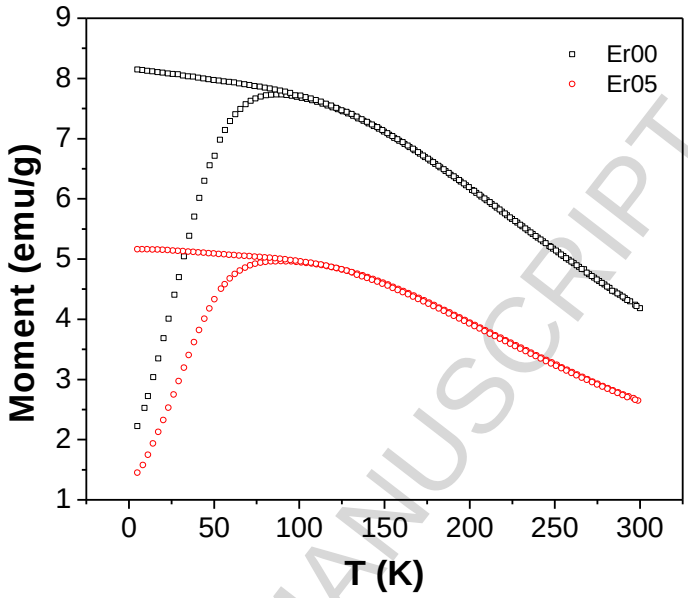

Figure 4. ZFC-FC curves for Er00 and Er05 MNPs, measured in 100 Oe.

Hysteresis curves for both MNP types at 5 *K* and 300 *K* are presented in Figure 5. At 5 *K*, samples had a coercive field around 200 Oe, while it shrank to below 10 *Oe* at 300 *K*. Clearly, *SQUID* labels both MNP types as superparamagnetic at 300 *K*. A weighted Langevin fit was employed in order to deduce the magnetization saturation (M_S) at 300 K and average size of particles. A log-normal particle size distribution,

$$g_n(d,\sigma,D) = \frac{1}{\sqrt{2\pi}\sigma\frac{D}{\mathrm{d}}}\exp\left[-\frac{\ln\left[\frac{D}{\mathrm{d}}\right]^2}{2\sigma^2}\right] \quad (1),$$

was used. Here, d and σ represent coefficients of the log-normal distribution, and D is the diameter of the particle. The complete weighted Langevin function took the form:

$$M(B) = M_s \int g_n(d,\sigma,D)\left(coth\left(\frac{M_s\rho 1/6\pi D^3 B}{kT}\right) - \frac{kT}{M_s\rho 1/6\pi D^3 B}\right) dD \quad (2).$$

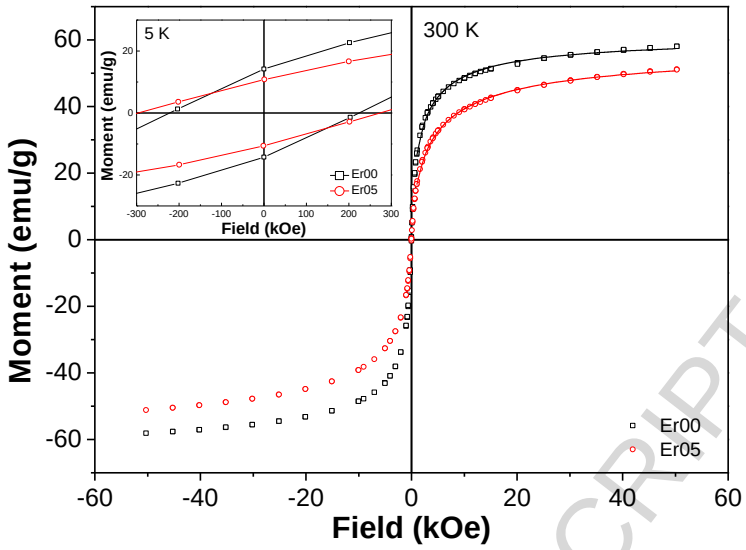

Figure 5. Hysteresis of Er00 and Er05 MNPs at 300 K. Lines represent weighted Langevin fits. Coercivity values at 5 K can be seen in the inset.

Particles were approximated as spheres with volume $V=1/6\ \pi D^3$. Density ρ was set to 5300 kgm^{-3}, which corresponds to the magnetite bulk value, kT represents thermal energy, and B is the magnetic flux density. Fitting parameters were d, σ and M_S. Expected MNP diameters d_{Lang} and standard deviations *std* were calculated using:

$$d_{Lang} = \int g_n(d,\sigma,D)DdD \text{ and } std = \sqrt{\int g_n(d,\sigma,D)D^2dD - (\int g_n(d,\sigma,D)DdD)^2}, \quad (3)$$

Final results are presented in Table 2. Derived average diameters showed excellent agreement with results of the *TEM* analysis and values acquired from *XRD* refinement.

Sample	M_S^{room}*(emu/g)*	d_{Lang} *(nm)*	D_{TEM} *(nm)*	D_{XRD} *(nm)*
Er00	60.9(2)	7(4)	7(2)	6.5(7)
Er05	57.3(2)	6(3)	6(1)	5.3(4)

Table 2. Values of the M_S and average diameter from weighted Langevin fit, TEM picture analysis and XRD refinement.

Binary ferrites (MFe_2O_4; M=Zn, Mn, Fe, Ni, Cr) and magnetite have often been doped/substituted with RE in order to improve their physical properties due to the large anisotropy of RE^{3+} moments [23] or structural defects induced by RE ions in the parent compound [24]. However, the effects of RE substitution in magnetite and ferrites are still not well understood. Our observed M_S value was slightly smaller in Er-substituted Fe_3O_4 MNPs (Er05) than in pure Fe_3O_4 MNPs (Er00)(Table 2). Consequently, from the magnetic point of view, the Er05 MNPs are deemed suitable for medical applications.

3.3. Cytotoxicity study

The cytotoxicity of Er05 MNPs was compared with that of naked Fe_3O_4MNPsusingtwo cell lines. Both MNP types exhibited cytotoxic effects on both cell lines when applied in high concentrations (500 *μg/ml*; data not shown). The IC_{50} values for Fe_3O_4 and Er05 MNPs were comparable in the case of normal lung fibroblasts, but the selectivity towards the melanoma cell line was different (Table 3). Internalization and distribution of the Er05 MNPs was consistently good and even throughout the cell lawn (Figure S1). Fe_3O_4MPNswere 2.5 times more toxic towards the melanoma cell line, while Er05 MNPs were 3 times less toxic towards the same cell line. This could be due to the specific microenvironment (slight pH differences) that may be present in the cancer cell line.

MNP type	*MRC5 (lung fibroblasts)*	*A375 (melanoma)*
Naked Fe_3O_4	50 ± 4	20 ± 2
Er05	45 ± 6	150 ± 9

Table 3. Cytotoxic activity of naked Fe_3O_4 and Er05 MNPs on human lung fibroblasts and melanoma cell line expressed as IC_{50} values (μg/ml). IC_{50} values correspond to nanoparticle concentrations which inhibited 50% of cell growth during 48 h of treatment (mean ± SD).

3.4. Ecotoxicity study: embryotoxic influence of Er05 MNPs on zebrafish (*Danio rerio*)

Zebrafish embryos were used to test the potential toxic effects of Er05 MNPs. Zebrafish (*Danio rerio*) are an excellent *in vivo* model for physiologically relevant whole-organism and behavior-based screening, which cannot be achieved with conventional *in vitro* systems [25]. Zebrafish embryos were developed in suitable medium containing 5 *μg/ml*, 10 *μg/ml*or50 *μg/ml* of MNPs, in 3 *ml* volumes.

MNP suspensions exerted no toxic effects on zebrafish embryos, even at the highest concentration examined (50 *μg/ml*). At this concentration, neither embryo mortality, nor any developmental defect, nor hatching delay was detected (Fig. 6). Furthermore, no signs of cardio- or neurotoxicity were observed (Fig. 6).

Nanoparticle aggregation was observed after 72 *h* incubation at 50 *μg/ml* (Fig. 6), and therefore, in order to rule out the possibility that the MPNs had aggregated and did not have the chance to exert harmful effect on zebrafish embryogenesis, *ICP-MS* analysis of treated and washed embryos was conducted. Special care was taken to avoid chorion material in the sample preparation for the *ICP-MS* analysis. Uptake of MNPs by zebrafish embryos was studied by both *ICP-MS* techniques. Results are presented in Table 4.

Sample	*Mass of MNPs calculated by measuring Er concentration(µg)*
Er05 - zebrafish; (50 *µg /ml*)	19.51
Er05 - ISO water; (50 *µg /ml*)	76.20

Table 4. Results of ICP-MS measurements: masses of MNPs in 1g zebrafish and in 3ml ISO water were shown.

The mass of Er05 MPNs in zebrafish was calculated by measuring Er masses using *ICP-MS*. *ICP-MS* revealed that MNPs were internalized in the embryos treated with them. Consequently, it was concluded that the MPNs, which had displayed a slight antiproliferative effect on lung fibroblast and melanoma cell lines, were not toxic for zebrafish embryos indicating their biosafety and potential application.

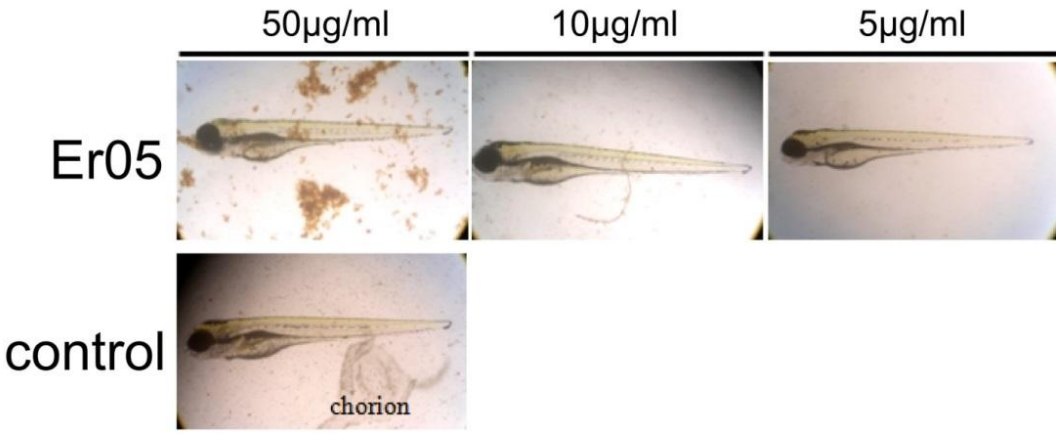

Figure 6. Morphology of the zebrafish (Danio rerio) embryos 96 h after treatment with three concentrations ofEr05 MNPs.

3.5. Radiolabeling of Er05MNPs with ^{90}Y and *in vitro* stability studies

The radiotracer method, readily and efficiently used in the MNP biodistribution study, firstly required optimization of the radiolabeling itself, to ensure that modification of the MNPs did not occur, which would have let to misinterpretation of the biodistribution results.

The highest radiolabeling yield for ^{90}Y-labeled Er05 MNPs, achieved under the experimental conditions previously described, was 89%, as detected by ITLC-SG and 92% determined by magnetic precipitation. Even a small amount of free $^{90}Y^{3+}$ present in the suspension could rapidly accumulate in bone, thus giving false results, and therefore, the magnetite precipitate was intensely washed several times with deionizied water to remove excess, unbound $^{90}Y^{3+}$.

After 72h of incubation, ^{90}Y-labeled Er05 MNPs demonstrated very high stability in saline and human serum (94.1 % and 92.7%, respectively),which can be attributed to the strong binding of $^{90}Y^{3+}$ by negatively charged carboxylate groups present on the surface of Er05 MNPs. At physiological *pH*, agglomeration of the radiolabeled Er05 MNPs was not observed during 3 days. Carboxylic groups on the surface of ^{90}Y-labeled Er05 MNPs provided significant electrostatic repulsion between the nanoparticles, resulting in excellent solubility and stability of ^{90}Y-labeled Er05 MNPs in aqueous solution as well as in physiological saline, human serum and *in vivo*.

3.6. Comparative biodistribution study of ^{90}Y-labeled Er05 MNPs by radiotracer technique and *ICP-MS*

The biodistribution of ^{90}Y-labeled Er05 MNPs was examined 30 minutes after intravenous injection in the animal model, healthy male Wistar rats, by two methods: radiotracer

and *ICP-MS*. Using the radio-tracer method, accumulation of MNPs in organs was quantified by measuring the radioactivity of bound radionuclides, while for the *ICP-MS* method, Er in the nanoparticle cores was measured. Radioactivity measurements of dissected tissues showed accumulation of ^{90}Y-labeled Er05 MNPs mostly in the liver (75.33% *ID*), followed by lungs (16.70% *ID*) and spleen (2.83% *ID*), while the remaining ^{90}Y-labeled Er05 MNPs were spread across the rest of the body (Figure 7).Such distribution is expected because nanoparticles of this size rapidly clear from the systemic circulation, predominantly by action of the liver and spleenic macrophages [26,27].An insignificant amount of radioactivity (0.44% *ID*) was detected in femur, a target organ for free ^{90}Y, indicating that ^{90}Y was tightly attached to the MNPs. Lungs, liver, spleen and blood were selected for further *ICP* analysis. Measured concentrations of Er in prepared tissue samples were (in *μg*/organ): lung (49.32), spleen (13.13), liver (264.01) and blood (1.07 *μg/ml*). Results of the radiotracer technique and *ICP-MS* spectroscopy are presented in Figure 8. In order to compare the results of these two methods, the percentages acquired by the radiotracer technique for four selected tissues were scaled so that their sum equaled 100%. *In vivo* stability of ^{90}Y-labeled Er05 MNPs was proved by *in vivo* retention of radioactivity in the liver, as well as by the constant amount of Er detected over time. This study demonstrates the unique advantages of the radiotracer technique: high sensitivity and simplicity. Although the *ICP* method enables detection of trace amount of elements in animal bodies, this measurement method suffers from low specificity due to inability to distinguish between endogenous elements and MNPs. The *ICP-MS* method using Er as a tracer proved to be a reliable method for quantifying accumulation of radiolabeled MNPs in blood and organs *in vivo*. Finally, our results show very good agreement between these methods and their combined application in our biodistribution study of ^{90}Y-labeled Er05 MNPs, providing additional credibility to these results.

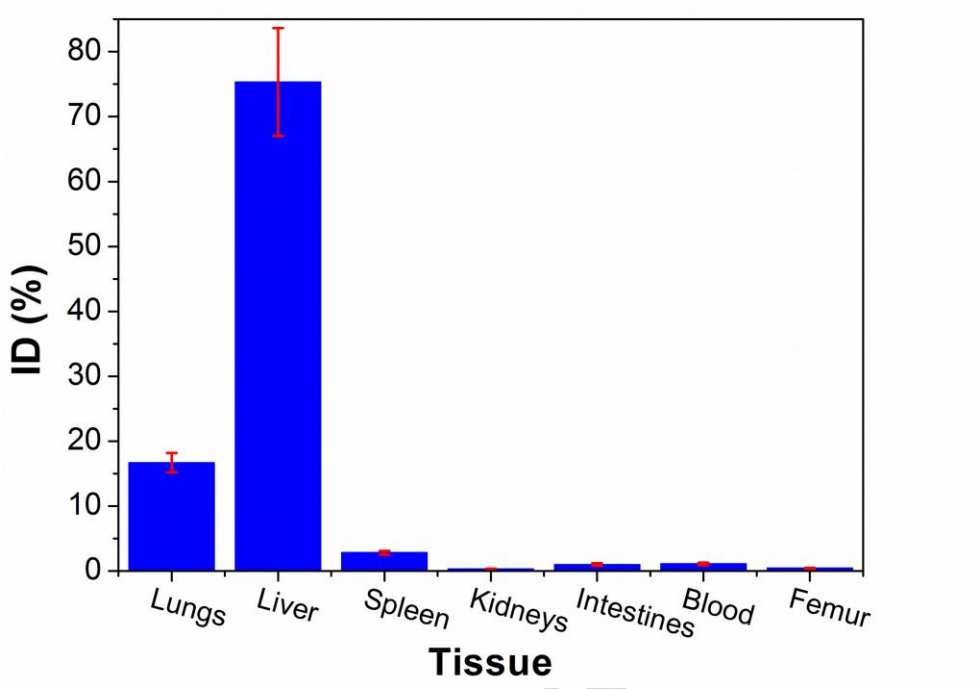

Figure 7. Biodistribution of ^{90}Y-labeled Er05 MNPs in rats using the radiotracer technique.

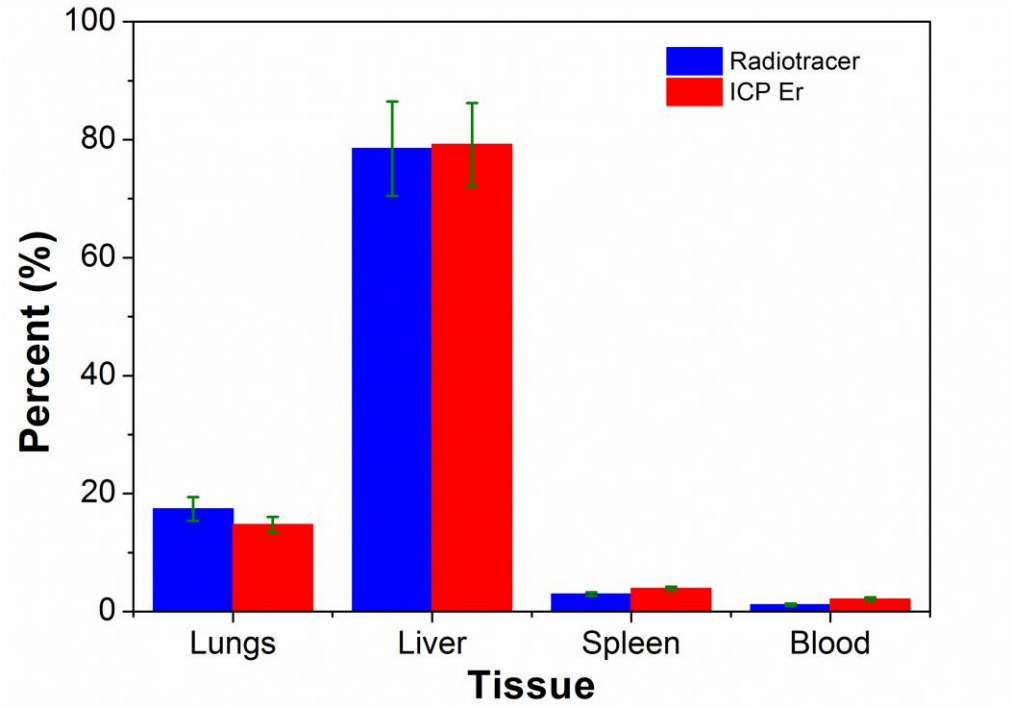

Figure 8. Comparative biodistribution of ^{90}Y-labeled Er05 MNPs using the radiotracer technique and ICP-MS. Radiotracer technique results for four tissues were scaled to 100% in order to compare them with ICP-MS results.

4. Conclusion

The $Fe_{3-x}Er_xO_4$ (x=0 and 0.05) citric acid coated nanoparticles synthesized using the modified Massart's method displayed high magnetic moments. Cytotoxicity analysis of Er05 citric acid coated and naked Fe_3O_4 MNPs indicated that the surface of the MNPs was non-toxic, while the toxicological test using zebrafish embryos pointed to the non-toxicity of the cores of the MNPs produced. In addition, *ICP-MS* showed that the MNPs entered the embryos and normal embryonal development ensued, so the particles are indeed non-toxic *in vivo*. The combination of the investigated toxicology test and the *ICP-MS* technique is an effective, fast, low cost and reliable method for *in vivo* toxicological studies.

MNPs labeled with radionuclide yttrium, ^{90}Y-Er05 MNPs, were obtained in a high radiolabeling yield and exhibit high *in vitro* and *in vivo* stability. Two complementary techniques, radiotracer and *ICP-MS*, supported each other, showing similar results of uptake in different *in vivo* rat tissues. Combined application of these methods should greatly enhance the reliability of studies into the biodistribution of MNPs in *in vivo* organs and tissues, and could be readily used for investigating organ and/or tissue distribution of MNPs potentially delivering a range of therapeutics. Additionally, biocompatible Er05 MNPs labeled with ^{90}Y are promising candidates for combined radionuclide-hyperthermia therapy.

Acknowledgment

The Ministry of Education, Science and Technological Development of the Republic of Serbia supported this work financially through the Project Grant No. III45015. The work of Y. M. and H.Z. was supported by International S&T Cooperation Program of China

(2015DFG52020). JNR was partially supported by OI173048 (MSTD, Republic of Serbia).The author thanks Dr. Biljana Dojcinovic for helpful discussions concerning ICP-MS results and for help to perform ICP-MS experiments. Structural characterizations have benefited from x-ray diffraction data collected at X17A beam line of the National Synchrotron Light Source at Brookhaven National Laboratory. ESB acknowledges Milinda Abeykoon for help with x-ray data collection. Nanoparticle structural characterization work at Brookhaven National Laboratory was supported by the US DOE, Office of Science, Office of Basic Energy Sciences (DOE-BES), under Contract No. DE-SC00112704.

References

[1] A.-H. Lu, E. L. Salabas and F. Schuth. Magnetic nanoparticles: synthesis, protection and application. *Angew. Chem. Int. Ed. Engl*.46, 1222 (**2007**).

[2] L. Cao, Y. Liang, F. Zhao, X. Zhao and Z. Chen. Chelerythrine and Fe_3O_4 Loaded Multi-Walled Carbon Nanotubes for Targeted Cancer Therapy. *J. Biomed. Nanotechnol.*12, 1312 (**2016**)**.**

[3] M. Colombo, S. Carregal - Romero, M. F. Casula, L. Gutierrez, M. P. Morales, I. B. Bohm, J. T. Heverhagen, D. Prosperi and W. J. Parak. Biological applications of magnetic nanoparticles. *Chem. Soc. Rev.* 41, 4306 (**2012**)**.**

[4] F. Liu, Y. Hou and S. Gao. Exchange-coupled nanocomposites: chemical synthesis, characterization and applications. *Chem. Soc. Rev.*43, 8098 (**2014**).

[5] R. Hao, R. Xing , Z. Xu , Y. Hou, S. Gao and S. Sun. Synthesis, functionalization, and biomedical applications of multifunctional magnetic nanoparticles. *Adv.Mater*.22, 2729 (**2010**).

[6] G. F. Goya, V. Grazu and M. R. Ibarra. Magnetic nanoparticles for cancer therapy. *Current Nanoscience* 4, 1 (**2008**).

[7] P. Tartaj, in Encyclopedia of Nanoscience and Nanotechnology Vol.6 (ed: H. S. Nalwa, American Scientific Publishers, USA 2004, pp. 822-831.

[8] A. Ruiz, Y. Hernandez, C. Cabal, E. Gonzalez, S. Veintemillas-Verdaguer, E. Martınez and M. P. Morales. Biodistribution and pharmacokinetics of uniform magnetite nanoparticles chemically modified with polyethylene glycol. *Nanoscale* 5, 11400 (**2013**)**.**

[9] S. Smulders, A. Ketkar-Atre, K. Luyts, H. Vriens, S. D. Nobre, C. Rivard, K. Van Landuyt, S. Baken, E. Smolders, L. Golanski, M. Ghosh, J. Vanoirbeek, U. Himmelreich

and P.H. Hoet. Body distribution of SiO_2-Fe_3O_4 core-shell nanoparticles after intravenous injection and intratracheal instillation. *Nanotoxicology* 10, 567 (**2016**).

[10] M. Varna, Ph. Ratajczak, I. Ferreira, C. Leboeuf, G. Bousquet and A. Janin. *In Vivo* Bistribution of Inorganic Nanoparticles in Preclinical Models. *J. Biomater. Nanobiotechnol.*3, 269 (**2012**).

[11] H. W. Zhao, S. H. Wang, S. N. Nguyen, S. G. Elci and I. A. Kaltashov. Evaluation of Nonferrous Metals as Potential *In Vivo* Tracers of Transferrin-Based Therapeutics. *J. Am. Soc. Mass Spectrom.* 27, 211 (**2016**)**.**

[12] S. H. Crayton, D. R. Elias, A. A. Zaki, Z. Cheng and A. Tsourkas. ICP-MS analysis of lanthanide-doped nanoparticles as a non-radiative, multiplex approach to quantify biodistribution and blood clearance. *Biomaterials* 33, 1509 (**2012**).

[13] M. Vucinic-Vasic, E. S. Bozin, A. Kremenovic, G. Stojanovic, U. Kozmidis-Luburic, M. Abeykoon, B. Jancar, A. Meden, L. Bessais and B. Antic. Thermal evolution of cation distribution/crystallite size and their correlation with magnetic state of Yb substituted Zn-ferrite nanoparticles. *J. Phys. Chem. C* 117, 12358 (**2013**).

[14] C. Tang, J. Edelstein, J. L. Mikitsh, E. Xiao, A. H. Hemphill II, R. Pagels, A.-M. Chackoand R. Prud'homme. Biodistribution and fate of core-labeled (125)I polymeric nanocarriers prepared by Flash Nano Precipitation (FNP). *J. Mater. Chem. B* 4, 2428 (**2016**).

[15] M. Radović, S. Vranješ-Đurić, N. Nikolić, D. Janković, G. F. Goya, T. Torres, P. Calatayud, I. Bruvera, R. Ibarra, V. Spasojević, B. Jančar and B. Antić. Development and evaluation of ^{90}Y-labeled albumin microspheres loaded with magnetite nanoparticles for possible applications in cancer therapy. *J. Mat. Chem.* 22, 24017 (**2012**)**.**

[16] R. Massart. Preparation of aqueous magnetic liquids in alkaline and acidic media. *IEEE Trans. Magn.* 17, 1247 (**1981**)**.**

[17] M. B. Hansen, S. E. Nielsen and K. Berg. Re-examination and further development of a precise and rapid dye method for measuring cell growth/cell kill. *J. Immunol. Meth.* 119, 203 (**1989**)**.**

[18] OECD, Test No. 236: Fish Embryo Acute Toxicity (FET) Test, OECD Publishing, Paris, 2013.

[19] M. Radovic, M. P. Calatayud, G. F. Goya, M. R. Ibarra, B. Antic, V. Spasojevic, N. Nikolic, D. Jankovic, M. Mirkovic and S. Vranjes-Duric. Preparation and in vivo evaluation of multifunctional 90Y-labeled magnetic nanoparticles designed for cancer therapy. *J. Biomed. Mater. Res. A*103, 126 (**2015**).

[20] R. D. Shannon and C. T. Prewitt. Effective ionic radii in oxides and fluorides. *Acta. Cryst.* B 25, 925 (**1969**).

[21] W. S. Rasband, ImageJ, U. S. National Institutes of Health, Bethesda, Maryland, USA, http://imagej.nih.gov/ij/, 1997-2014.

[22] L. D. Tung, V. Kolesnichenko, G. Caruntu, D. Caruntu, Y. Remond, V. O. Golub, C. J. O'connor and L. Spinu. Annealing effects on the magnetic properties of nanocrystalline zinc ferrite. *Physica B* 319**,** 116 (**2002**)**.**

[23] R. V. Upadhyay, A. Gupta, C. Sudakar, K. V. Rao, K. Parekh, R. Desai and R. V. Mehta. Effect of rare-earth Ho ion substitution on magnetic properties of Fe_3O_4 magnetic fluids. *J. Appl. Phys.* 99, 08M906 (3pp) (**2006**)**.**

[24] S. S. Laha, R. Regmi and G. Lawes. Structural origin for low-temperature relaxation features in magnetic nanoparticles. *J. Phys. D. Appl. Phys.* 46, 325004 (**2013**).

[25] Y. Peng, J. Li, Y. Sun, J. Y.-W. Chan, D. Sheng, K. Wang, P. Wei, P. Ouyang, D. Wang, S. M. Y. Lee and G.-C. Zhou. SAR studies of 3,14,19-derivatives of andrographolide on anti-proliferative activity to cancer cells and toxicity to zebrafish: an in vitro and in vivo study. *RSC Adv.* 5, 22510 (**2015**).

[26] S. M. Moghimi, A.C. Hunter and J. C. Murray. Nanomedicine: current status and future prospects. *FASEB J*. 19, 311 (**2005**).

[27] H. Arami, A. Khandhar, D. Liggitt and K. M. Krishnan. In vivo delivery, pharmacokinetics, biodistribution and toxicity of iron oxide nanoparticles. *Chem. Soc. Rev*. 44, 8576 (**2015**).

Graphical abstract

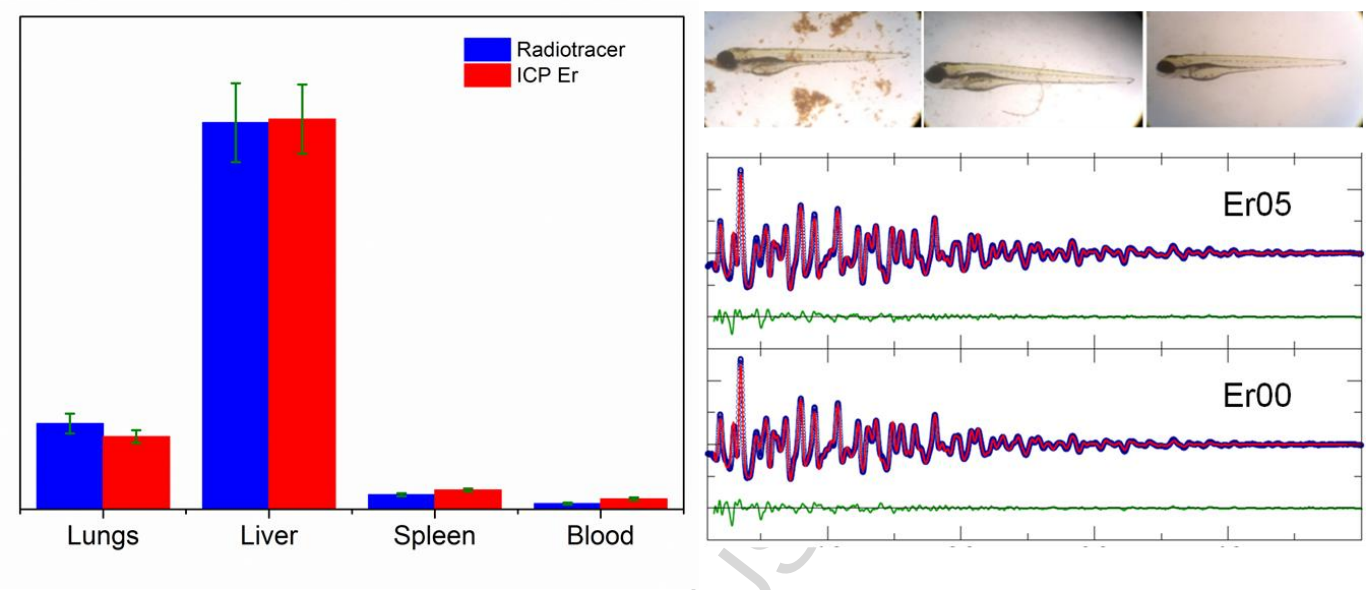

Highlights

- Citric acid coated $(Fe,Er)_3O_4$ MNPs were found to induce low toxicity both in human cell fibroblasts and in zebrafish (*Danio rerio*) embryos.

- MNPs labelled with radionuclide yttrium, ^{90}Y-$(Fe,Er)_3O_4$ MNPs, were obtained in high radiolabelling yield and exhibit high *in vitro* and *in vivo* stability.

- ^{90}Y-$(Fe,Er)_3O_4$ MNPs can be reliably used in bio-distribution studies to obtain accurate measurements.

- *ICP-MS* showed that MNPs do enter embryos, so particles are indeed *in vivo* non-toxic.

- Combined application of radiotracer and *ICP-MS* methods greatly enhance the reliability of studies into the biodistribution of MNPs in *in vivo* organs and tissues.

- The combination of the investigated toxicology test and the *ICP-MS* technique is an effective, fast, low cost and reliable method for *in vivo* toxicological studies.